HHS Public Access

Author manuscript

Mol Neurobiol. Author manuscript; available in PMC 2023 April 01.

Published in final edited form as:

Mol Neurobiol. 2022 April ; 59(4): 2605–2619. doi:10.1007/s12035-022-02760-3.

The putative *Drosophila* TMEM184B ortholog Tmep ensures proper locomotion by restraining ectopic firing at the neuromuscular junction

Tiffany S. Cho[*,1], **Eglė Beigaitė**[*,2], **Nathaniel E. Klein**[*,1], **Sean T. Sweeney**[2], **Martha R.C. Bhattacharya**[1,#]

[1]Department of Neuroscience, University of Arizona, 1040 E 4th Street, Tucson AZ 85721, USA

[2]Department of Biology, University of York, York, YO10 5DD, UK; York Biomedical Research Institute, University of York, York, YO10 5DD, UK

Abstract

TMEM184B is a putative seven-pass membrane protein that promotes axon degeneration after injury. *TMEM184B* mutation causes aberrant neuromuscular architecture and sensory and motor behavioral defects in mice. The mechanism through which TMEM184B causes neuromuscular defects is unknown. We employed *Drosophila melanogaster* to investigate the function of the closely related gene, *Tmep* (CG12004), at the neuromuscular junction. We show that Tmep is required for full adult viability and efficient larval locomotion. *Tmep* mutant larvae have a reduced body contraction rate compared to controls, with stronger deficits in females. In recordings from body wall muscles, *Tmep* mutants show substantial hyperexcitability, with many post-synaptic potentials fired in response to a single stimulation, consistent with a role for Tmep in restraining synaptic excitability. Additional branches and satellite boutons at *Tmep* mutant neuromuscular junctions are consistent with an activity-dependent synaptic overgrowth. Tmep is expressed in endosomes and synaptic vesicles within motor neurons, suggesting a possible role in synaptic membrane trafficking. Using RNAi knockdown, we show that Tmep is required in motor neurons for proper larval locomotion and excitability, and that its reduction increases levels of presynaptic calcium. Locomotor defects can be rescued by presynaptic knock-down of endoplasmic reticulum calcium channels or by reducing evoked release probability, further suggesting that excess

[#]Correspondence: marthab1@email.arizona.edu.
[*]These authors contributed equally.

Authors' contributions

S.T.S. and M.R.C.B. proposed the research and assisted in experimental design. T.S.C., E.B., and N.E.K. designed and performed experiments. All three first authors (indicated with *) made significant discoveries leading to this manuscript, resulting in all three being listed as equal first-authors. T.S.C. and M.R.C.B. wrote the manuscript, with editing by E.B. and S.T.S.

Conflicts of interest/Competing interests

The authors declare no competing financial interests.

Code availability

All code used in image analysis is deposited on our research group's GitHub page and is freely available to all (https://github.com/martharcb).

Consent for publication

All authors have had the opportunity to review this manuscript prior to submission, and all give their approval for publication of this work.

synaptic activity drives behavioral deficiencies. Our work establishes a critical function for *Tmep* in the regulation of synaptic transmission and locomotor behavior.

Keywords

TMEM184B; neuromuscular junction; excitability; synapse; epilepsy; calcium

Introduction

Synaptic transmission at the neuromuscular junction (NMJ) requires precisely controlled anatomical and functional coordination between motor neuron terminals and their postsynaptic muscle partners. When action potentials arrive at synaptic terminals, calcium rise in the presynaptic terminal evokes the fusion of neurotransmitter-filled vesicles with the plasma membrane, triggering depolarization of muscle fibers. To fire a single action potential, the synaptic terminal must be able to restore ion levels to pre-stimulus levels quickly [1]. Mutations that fail in clearance of synaptic calcium [2], cause gain of function of calcium channels [3], or cause loss of the repolarizing function of potassium channels [4], show ectopic firing of synapses. This has deleterious effects on neural circuits and their resulting behavioral outputs.

The trafficking of presynaptic membrane proteins to their proper locations underlies the efficiency of synaptic transmission. Mutations that impair endocytic recycling of proteins leave presynaptic terminals ill prepared for repetitive firing events [5–9]. In addition, lipid dynamics at the synapse contribute to proper firing patterns [10–12]. Endosomes serve as sorting stations at the synapse and participate in the synaptic vesicle recycling process across species [5, 13–15]. The perturbation of vesicle recycling via the manipulation of membrane trafficking has been suggested as a therapeutic strategy for synaptic disorders [16].

The *TMEM184B* gene is a predicted 7-pass transmembrane protein that localizes to endosomal compartments, suggesting a possible role in intracellular membrane trafficking [17]. TMEM184b promotes efficient axon degeneration following nerve injury [17]. Paradoxically, *TMEM184B* mutations also cause substantially swollen nerve terminals, including at the NMJ. Mice deficient in TMEM184b show both sensory and coordination defects, indicating an important contribution to neuron function even in the absence of injury [17, 18]. Despite its clear contribution to synaptic architecture and behavior, its function at the synapse is not understood.

We sought to learn how TMEM184B influences synaptic structure and function using the *Drosophila* neuromuscular junction, a model glutamatergic synapse in an easily accessible system for structural, functional, and behavioral analysis. We have thus investigated the function of the predicted *Drosophila* ortholog of *TMEM184B*, *CG12004*, which we named *Tmep* (transmembrane endosomal protein). Here we show that loss of Tmep, like TMEM184B, causes structural defects at the NMJ and impairs locomotion. Flies deficient in Tmep show striking hyperexcitability at the NMJ, with many ectopic responses to a single stimulus. Despite broad expression, Tmep seems to control behavioral output via its motor neuron activity. Tmep reduction results in a higher density of presynaptic active

zones and elevated baseline synaptic calcium. Correspondingly, behavioral deficits caused by Tmep reduction can be rescued by depression of synaptic excitability through multiple mechanisms. Our data supports a presynaptic contribution of the TMEM184B ortholog Tmep in regulation of synaptic function and motor behavior.

Results

CG12004 (Tmep), the predicted *Drosophila* ortholog of TMEM184b, is needed for full viability and locomotor function

To identify the closest ortholog to mouse and human TMEM184B, we used NCBI BLAST to select the most similar proteins in *Drosophila*. The CG12004 gene is 56% identical and 65% similar at the protein level to human TMEM184B, and reverse blast of CG12004 identifies TMEM184B as its closest relative (96% query coverage, E value $7e^{-168}$). This is consistent with predictions using NCBI Homologene, indicating that CG12004 and TMEM184B are homologs (not shown). To understand which domains are most conserved, we mapped the aligned sequences onto the predicted transmembrane structure of CG12004. Two isoforms of CG12004 are predicted which differ only at their C-terminal (Fig 1a–b). The 7-pass transmembrane region, which has distant similarity to bile acid transporters, shows 71% amino acid identity and 82% similarity between fly CG12004 and human TMEM184B, indicating strong evolutionary conservation (Fig 1a). The third transmembrane domain is less strongly predicted than others (TM3 shows 70% probability, while all others show 95% probability or greater, based on TMMHM-2.0 Server analysis) but appears as a hydrophobic peak in all orthologs. Domains outside of the membrane are less well conserved, but a stretch of the membrane-proximal C-terminal shows high homology (67%, or 36 of 54 amino acids identical across all species), while the N-terminal is only 26% identical. Based on this analysis, CG12004 is likely to be the ortholog of mouse and human TMEM184B. Because TMEM184B localizes to endosomal compartments in cultured mammalian neurons [17], we have named the *Drosophila* isoform Tmep (Transmembrane endosomal protein).

We used homologous recombination to create a Tmep mutant allele, $Tmep^{Ex}$, with a 16-base excision (bases 20–35 in the open reading frame) that is predicted to create a nonsense mutation 7 amino acids from the N-terminal, affecting both the short and long Tmep isoforms (Fig 1b). We also obtained a second allele ($Tmep^{Cri}$) in which Tmep was disrupted by a CRISPR-Mediated Integration Cassette (CRIMIC) cassette containing a splice acceptor, *GAL4* sequence, and a “stop” signal [19]. Both $Tmep^{Ex}$ and $Tmep^{Cri}$ disrupt all four predicted *Tmep* transcripts. We used these two alleles in transheterozygous combination with a deficiency, *Df(3L)Exel6087*, that uncovered the *Tmep* locus, as well as two RNAi constructs targeting different conserved sequences (Fig 1b), in our subsequent studies.

When setting up transheterozygous crosses to study *Tmep* mutant flies, we observed that $Tmep^{Cri}$/Df flies had severely impaired rates of eclosion compared to non-mutants in the same vial (0.057+/− 0.10 (mean, SD) of expected ratio in females, 0.67 +/− 0.27 of expected in males) (Fig. 1c). *Tmep*-associated lethality was greater in females than in males. This lethality is often observed prior to wandering third-instar stage, as relatively few mutant larvae with this allele combination can be found (not shown). In both sexes, Tmep

re-expression driven by the *CRIMIC-GAL4* (here used as both a mutant allele and a rescue driver in the Tmep expression pattern) was sufficient to rescue eclosion rates to wild type levels (0.90 +/− 0.099 (mean, SD) of expected ratio in females, 1.16 +/− 0.23 of expected in males) (Fig. 1c). Due to the severe lethality of $Tmep^{Cri}$/Df, we analyzed $Tmep^{Ex/Df}$ in subsequent experiments.

Because *Tmem184b* mutant mice show sensory and motor defects [17, 18], we wanted to know if *Tmep* mutant flies would show similar phenotypes. First, we evaluated if adult flies showed impaired motor function. In a climbing assay, *Tmep* mutant females showed slower climbing time after disorientation, while males were not affected (Fig 1d). In larvae, we assessed how *Tmep* reduction impacted locomotor behavior using a simple crawling assay. In females, both $Tmep^{Ex}$ and $Tmep^{Cri}$, in trans to a deficiency, showed reduced body contraction (crawling) rates compared to controls (Fig. 1e), with $Tmep^{Cri}$ having stronger effects (for $Tmep^{Ex}$/Df, 33.5 +/− 3.4 (SD) contractions/min; for $Tmep^{Cri}$/Df, 21.6 +/− 14.4 (SD)). Re-expression of *Tmep* driven by *CRIMIC-GAL4* was sufficient to rescue crawling behavior in females (47.7 +/− 9.5 (SD) contractions/min) (Fig. 1e). In males, while behaviors trended similarly to females, none of the *Tmep* mutant genotypes were significantly different from wild type ($Tmep^{Ex}$/Df, 37.4 +/− 3.3 (SD) contractions/min; $Tmep^{Cri}$/Df 42.0 +/− 9.7 (SD); rescue, 48.3 +/− 11.3(SD)) (Fig 1f). Taken together, our data show that Tmep expression is critical for viability and behavior, with effects of Tmep reduction more deleterious in females. We do not yet know the basis for the sexual dimorphism in *Tmep* mutants. In subsequent experiments, we separated animals by sex to fully capture the phenotypes caused by Tmep reduction.

Tmep localizes to endosomes and synaptic vesicles in motor neurons

TMEM184B is expressed in motor and sensory neurons as well as in the brain in mice, starting from early development [18]. To understand why *Tmep* mutant larvae show hyperexcitability, we first wanted to establish its overall expression pattern at the larval stage. We developed a polyclonal antibody to *Drosophila* Tmep (regions used as antigens shown by red lines in Fig 1a). Tmep is expressed in a punctate pattern in the neurons of the ventral nerve cord (Fig. 2a). Importantly, we see very low signal in $Tmep^{Ex/Df}$ larvae, indicating that our antibody is specific. Tmep protein is also found at low levels at the NMJ (Fig. 2b).

We wanted to evaluate if, as in mice, Tmep is found on Rab11-positive recycling endosomes. Using an mKate-tagged Tmep transgene, we found a similar punctate, vesicular pattern as seen with the Tmep antibody. These small Tmep-positive puncta showed partial overlap with larger, Rab11-positive areas in motor neuron cell bodies (28 +/− 8% (SD) of Tmep is found colocalized with Rab11+ areas, calculated by Manders correlation coefficient) (Fig 3c). In addition to direct overlap, Tmep puncta were often adjacent to Rab11-positive puncta, suggesting that Tmep-positive compartments may at least transiently intersect with Rab11-positive endosomes (Fig 3c'). We also observed substantial overlap between mKate-Tmep and GFP-tagged neuronal Synaptobrevin (n-Syb) (43 +/− 20% (SD) overlap, Mander's coefficient) (Fig 3d–d'), which is localized to synaptic vesicles as well as synaptic endosomal compartments [20]. Taken together, our data indicate that Tmep is

primarily expressed on intracellular membranes, including partial localization to endosomes and synaptic vesicles. This localization is consistent with a role in endomembrane function in neurons.

We also took advantage of the Tmep-*CRIMIC-GAL4* insertion to express nuclear-localized RFP in cells expressing endogenous Tmep. Tmep is expressed in muscle and motor neurons, but not in glia in the larval brain (Online Resource 1a–b). We also observe Tmep expression in the gut and fat bodies (Online Resource 1c–d). These data indicate that Tmep is broadly expressed in *Drosophila* larvae.

Tmep mutant larvae show morphological defects at the neuromuscular junction

Tmep locomotor phenotypes in *Drosophila* larvae could be caused by morphological changes at the synapse, alterations in synaptic signaling pathways, impaired excitability, or a combination. To investigate if changes in NMJ morphology could contribute to phenotypes, we examined terminal morphology with immunohistochemistry. In mice, disruption of TMEM184B expression causes swellings in the NMJ [17]. In *Drosophila*, we observed statistically significant increase in nerve terminal branching in *Tmep* mutant female larvae (Fig 3a–b). Satellite or fragmented bouton architecture is observed at the ultrastructural level (Fig 3c) in addition to the light level (Fig 3d–e). The presence of satellite boutons has been previously linked to greater active zone density [21], so we quantified active zones using an antibody to Bruchpilot, an active zone protein. We identified a significant increase in active zones in the boutons of Tmep mutant females (Fig 3f–g). Taken together, our results indicate that Tmep is required for NMJ structure (a result consistent with observations made at the mouse NMJ) and suggest that morphological changes could contribute to *Tmep* phenotypes [17].

Tmep restrains ectopic firing at neuromuscular junctions

The presence of increased active zones as well as the behavioral impairments led us to wonder whether synaptic transmission at the neuromuscular junction is altered by the lack of Tmep. Impaired locomotion can be caused by mutations in ion channels and other pathways that affect synaptic transmission and nerve excitability [22]. In mice, *Tmem184b* mutation affects performance on broad sensorimotor tests, but does not alter conduction velocity or action potential amplitude in sensory or motor nerves [17]. Therefore, we hypothesized that Tmep loss may impact synaptic transmission rather than action potential propagation, leading to behavioral defects. To investigate whether Tmep is required for proper synaptic transmission, we recorded both spontaneous (mini excitatory junctional potential, mEJP) and evoked (EJP) activity in 3rd instar larvae. In wild type larvae, a single evoked action potential triggers a single EJP spike. However, when action potentials were triggered in $Tmep^{Ex}$/Df larvae, we saw a striking hyperexcitability phenotype (Fig 4a). Both males and females commonly responded more than once to a stimulus, and occasionally a single stimulus induced over 20 EJPs over the 5 second post-stimulus period (Fig 4b). While the first EJP did not vary in amplitude between wild type and mutants (Fig 4c), all second (ectopic) EJPs had significantly reduced amplitudes in comparison to the first response (Fig 4d–e). Ectopic EJPs occurred relatively rapidly after the stimulus, with spacing between ectopic responses lengthening slightly by the 5th response (Fig 4f). When examining

spontaneous events (mEJPs), we found a reduction in the amplitudes of mEJPs in female, but not male, *Tmep* mutants (Fig 4g). These data show that Tmep normally restrains evoked synaptic responses. Taken together with the behavioral data, our recordings support a model where, in the absence of Tmep, excessive firing at NMJs impairs locomotor ability.

Tmep is required presynaptically for neuromuscular phenotypes

Tmep is expressed both by motor neurons and muscle. To establish where it contributes to locomotor function and physiology, we used tissue-specific RNA interference. When we recorded EJPs from larvae with presynaptic Tmep knockdown, we observed a subtle but persistent multi-peak EJP in response to the majority of evoked stimuli (Fig 4h). Ectopic EJPs fully independent of evoked stimuli were rare but did occur in some larvae. We also evaluated the effect of Tmep knockdown on larval behavior. Consistent with the electrophysiological effects, we observed a reduction in larval crawling rate when Tmep is knocked down pre-synaptically (*Vglut-GAL4*) using two independent Tmep RNAi transgenes (Fig 4i). The behavioral impairment is similar to what we measured in genetic mutants (Fig 1e). The effect of knockdown is observed in both male and female larvae. Knockdown of Tmep in muscle (using *MHC-GAL4*) does not impair crawling; surprisingly, it increases contraction rate, indicating a possible feedback mechanism at play (Fig 4i). These data support a primarily presynaptic function for Tmep in controlling synaptic transmission and motor function.

Larval crawling deficiencies are restored by reduction of presynaptic excitability

Ectopic EJPs are seen in *Drosophila* mutants that impair the clearance of calcium from presynaptic terminals [2, 3]. To evaluate calcium levels in presynaptic terminals, we expressed the calcium sensor GCaMP5G along with tdTomato (which fills the terminal) in motor neurons. This transgene (UAS-GCaMP5G-T2A-tdTomato) allows ratiometric calculations, minimizing focal artifacts [23]. When Tmep was knocked down, larvae had elevated presynaptic calcium compared to GAL4 only controls (Fig 5a–b). This result is consistent with the electrophysiological data and suggests that high levels of presynaptic calcium are contributing to our phenotypes. To test whether this is the case, we asked if reducing cytoplasmic calcium levels specifically in motor neurons could improve Tmep-knockdown locomotor behavior. The endoplasmic reticulum and its stored calcium positively influence synaptic transmission [24, 25]. We first blocked store-operated calcium release in two ways, using neuron-specific RNAi to either the inositol triphosphate (IP_3) receptor (ITPR) or the ryanodine receptor (RyR). While the individual RNAi's to each receptor did not change baseline locomotion, both ITPR and RyR knockdown were able to restore normal locomotor activity in the background of *Tmep* RNAi (Fig 5c–d). This fits with the emerging roles for presynaptic ER signaling in the regulation of synaptic transmission [26–28].

We also dampened presynaptic activity using an orthogonal strategy. The NAD+ synthetic enzyme NMNAT restrains evoked synaptic transmission in mutants where synaptic activity is enhanced, such as *highwire* (*hiw*) [29]. In addition, over-expression of NMNAT in a wild type background dampens evoked release from motor neurons [29]. Indeed, we found that by driving additional NMNAT expression in motor neurons in a Tmep RNAi background,

crawling behavior was restored to control levels (Fig 5c–d). While our data does not definitively prove that NMNAT is directly regulated by Tmep (and indeed, NMNAT has many functions including maintenance of axon viability [30–32]), it supports the hypothesis that presynaptic hyperexcitability is the cause of crawling deficiencies in Tmep mutant and knockdown larvae.

Our data support a model in which Tmep, working in an endosomal or vesicular compartment, influences excitability through the regulation of calcium levels at presynaptic terminals. While the source of the additional calcium is unknown, additional active zones per bouton may contribute to this phenotype. In Tmep mutants, excess calcium and the resulting ectopic firing may cause activity-dependent synaptic overgrowth, which results in the appearance of additional boutons and branches. Together, these impairments reduce the coordination of muscle contractions necessary for larval locomotion (Fig 5e).

Discussion

In this work we have identified a role for Tmep in promoting proper neuromuscular junction architecture as well as restraining ectopic firing at the glutamatergic synapses of the *Drosophila* NMJ. Excessive synaptic activity can result in epileptic syndromes. In epilepsy, excitatory-inhibitory balance is often disrupted in favor of over-excitation [33, 34]. Our data indicate that Tmep acts presynaptically to ensure both the architecture of the NMJ and the proper responses to nerve stimulation. Interestingly, we have recently identified human patient variants in *Tmem184b*, one of which causes myoclonic epilepsy as well as other neurological syndromes (K. Chapman and S. Berger, personal communication). We hope to delve further into the links between Tmem184b structure, function, and excitability in the future by analyzing the effect of known patient variants on the phenotypes we describe in this manuscript.

While we do not yet precisely know the nature of Tmep's contribution to synaptic hyperexcitability, we speculate that it controls a membrane trafficking function at the presynaptic terminal. We found that Tmep, like mouse TMEM184B [17], is localized to endosomal compartments. Interestingly, we see significant co-localization of Tmep with n-Syb, a protein present on both endosomes and synaptic vesicles. Loss of n-Syb causes the accumulation of endosomes [20], a phenotype reminiscent of the endolysosomal accumulations seen in mouse *TMEM184B* mutants. Along with the role of the yeast ortholog Hfl1 in vacuolar degradation [35, 36], these data implicate Tmep and its family members in endolysosomal function.

Tmep would thus join a group of endosomal and membrane trafficking effectors whose mutation impairs synaptic transmission. For example, Rab5 promotes efficient release of synaptic vesicles by ensuring proper membrane exchange between these vesicles and synaptically localized endosomes [13, 37]. In addition, mutations in the NPC1 gene that cause Niemann-Pick type C1, a fatal neurodegenerative disease caused by faulty lysosomal-ER cholesterol transfer, also show ectopic responses to presynaptic stimulation [12]. These studies underscore the need to regulate membrane trafficking to ensure proper responses to stimulation. A priority for future work should be to investigate how Tmep and related

mammalian proteins influence essential functions of endosomes, lysosomes, and synaptic vesicles at neuromuscular junctions.

Our data suggest that Tmep is important to restrict the amount of cytosolic calcium in the presynaptic terminal. Without this layer of regulation, excess calcium may be causing both ectopic firing as well as synaptic overgrowth phenotypes. Four pieces of evidence support this assertion. First, our data shows elevated cytosolic calcium in the presynaptic boutons of Tmep knockdown larvae. Second, we see an increased active zone density, as measured by BRP, in *Tmep* mutant boutons. BRP is known to recruit the voltage-gated calcium channel Cacophony (Cac) to active zones and also provides more sites for the modulator CaMKII to localize to sites of release [38–40]. Therefore, excess BRP in *Tmep* mutants may facilitate additional calcium entry into terminals. Third, reducing presynaptic calcium with knockdown of store-operated calcium channels reverses behavioral deficits in Tmep RNAi larvae. IP3R and RyR activity increases presynaptic calcium levels and correspondingly promotes synaptic vesicle exocytosis [41, 42]. The primary effect of IP3R and RyR function on transmission at synapses is through the promotion of calcium-induced calcium release and subsequent asynchronous firing (in mouse) [41, 43, 44], as well as in maintaining homeostatic plasticity (in flies) [45]. Therefore, ectopic EJPs in *Tmep* mutants could be presenting an increase in asynchronous firing due to a prolonged increase in presynaptic calcium [46]. Finally, in *Tmep* mutants we see an increase in branching and in satellite boutons per synaptic branch. It is well established that mutations in potassium channels such as *Shaker, Slo, and Seizure* cause activity-dependent synaptic overgrowth including the formation of satellite boutons, which can be suppressed by the introduction of sodium or calcium channel mutations in these mutant backgrounds [47–49]. Thus, our data support a model in which Tmep maintains appropriate levels of cytosolic calcium which prevents synaptic overgrowth and ectopic firing.

While our experiments were designed to examine cytosolic calcium, it is also possible that *Tmep* mutants have altered calcium in membrane-bound organelles. ITPR is expressed on the endoplasmic reticulum and plays specialized roles in loading calcium into compartments such as mitochondria [50] and lysosomes [51]. The accumulation of lysosomes in mouse TMEM184b mutants [17] is consistent with an alteration that disrupts their function, akin to a lysosomal storage disease-like condition. Lysosomes and other acidic organelles can act as a source of calcium, often via Twin-pore channels and NAADP action [52]. Loss of function of Tmep could also perturb plasma membrane calcium channel distribution via an endosomal function, in a similar manner to the role of Rab11 in N-type calcium channel recycling [53]. Another possibility is that Tmep assists in establishing or maintaining membrane contact sites to ensure proper calcium handling in membrane-bound organelles [54, 55]. Any disruption of calcium levels at the synapse would be predicted to cause changes in excitability, leading to the phenotypes we observe in *Tmep* mutants.

In many of our phenotypes, we document a difference in the strength of phenotypes between male and female larvae. For example, larval crawling phenotypes in *Tmep* mutants only trend towards deficient in males but are significantly altered in females. Interestingly, knockdown of Tmep specifically in motor neurons causes similar crawling dysfunction in both sexes, suggesting that the sex-specific penetrance of our phenotypes may not be

due to Tmep's role in motor neurons. In physiological tests, both male and female *Tmep* mutants show ectopic firing upon presynaptic stimulation, underscoring a more universal (non-sex-specific) role for Tmep in the neuron. Taken together, we hypothesize that a non-neuronal role for Tmep, perhaps in endomembrane trafficking, may contribute to the sexually dimorphic phenotypes.

In summary, we have discovered a role for the likely fly ortholog of *TMEM184B*, Tmep, in synaptic excitability and behavior. The evolutionary conservation between fly *Tmep* and human *TMEM184B* is high, suggesting a critical function across eukaryotic organisms. Our work establishes a system in which to study how Tmep and TMEM184B influence synaptic transmission and may contribute to nervous system disorders.

Materials and Methods

Fly stocks and husbandry

Flies were raised at 25°C, and all experiments were performed at 22°C. Fly stocks were from either the Bloomington Drosophila Stock Center (BDSC) or the Vienna Drosophila RNAi Consortium (VDRC) as follows: *Vglut*-GAL4 (BDSC # 24635), *Df(3L)Exel6087* (BDSC #7566), $Tmep^{Cri}$ (BDSC #91319), *MHC82*-GAL4 [56], UAS-CG12004 RNAi (TRP #57429), UAS-CG12004 RNAi (VDRC #101732), UAS-ITPR RNAi (BDSC #51795), UAS-RyR RNAi (BDSC #28919), UAS-NMNAT (BDSC # 39699), UAS-GcaMP5-T2A-TdTomato (BDSC # 80079) and wild type (Canton S or w^{1118}). $Tmep^{Ex}$ was made by InDroso Functional Genomics (Rennes, France) by homologous recombination to create a 16-base deletion in the first coding exon of CG12004. UAS-mKate:CG12004 (long form) and UAS-mKate:hTMEM184B (human) were created by cloning into the pBID vector, which was a gift from Brian McCabe (Addgene plasmid # 35190; http://n2t.net/addgene:35190; RRID:Addgene_35190). Injections were done at Bestgene (Chino Hills, CA).

Genome Alignment

Sequences were downloaded from NCBI as follows: human TMEM184b (isoform a, NP_036396.2), mouse TMEM184b (isoform 1, NP_766196.1). Fly orthologs were derived from Flybase (CG12004-RD is the long form, CG12004-RA is the short form). Alignments were done in Snapgene using ClustalW. Membrane regions were annotated manually based on membrane predictions using the TMHMM Server v 2.0 available at http://www.cbs.dtu.dk/services/TMHMM/.

Antibody generation

Drosophila Tmep cDNA was used as a template to generate PCR fragments corresponding to two selected peptide fragments of Tmep 1–67 (N-terminal) and Tmep 393–486 (C-terminal) using oligonucleotides (For a.a. 1–67: CF044–1F GGGGCCCCTGGGATCCATGAGCACAACCGCCGCCAG, CF044–1R GGGAATTCGGGGATCTTACTGGGCGGTCTTTGTCTGCAGfor a.a 393–486: CF044–4F GGGGCCCCTGGGATCCGGTGGCAAGAATTCCCGCGGCATTCCF044–4R GGGAATTCGGGGATCTTACTGGTACTCATCGTCGCTGCTC).

After amplification with KOD Hot-Start DNA polymerase (Novagen), the DNA was incubated in an InFusion (Takara Bio) reaction with *Bam*HI linearised pGEX-6p-3. The product was transformed into *E. coli* XL1-blue (Stratagene) and the sequence confirmed. The resulting constructs yielded an N-terminal fusion of GST to the CG12004 peptide sequences. The expression vector was transformed into *E. coli* Codon plus (DE3) (Stratagene) for expression studies. Overnight cultures containing LB, ampicillin (100μg/ml) were inoculated from glycerol stocks and incubated at 37°C and 200rpm. The cultures were then used to inoculate 500 ml of LB containing ampicillin (100μg/ml) before further incubation at 37°C and 200rpm. At a culture OD_{600nm} of 0.6Au, IPTG was added to a final concentration of 1 mM and incubation was continued at 18^{O}C and 200rpm for 20 hours. The induced culture was centrifuged at 7,000*g* for 10 min at 4°C before the supernatant was discarded and the pellet was stored at −80°C until required. The purification of GST-tagged protein was performed by affinity chromatography using the following procedure. Frozen cell pellets were thawed and resuspended in lysis buffer - PBS, pH 7.2 containing protease inhibitor cocktail (Roche), prior to disruption by sonication. The supernatant was then recovered by centrifugation at 35,000*g* for 10 min at 4°C and then filtered (0.2 μm). The crude extract was applied to 1ml Glutathione Sepharose beads (GE Healthcare) previously equilibrated in Buffer A (PBS) for 90min at 4°C. On completion of binding, the resin was washed three times with 50 bed-volumes (CV) of Buffer A before isocratic elution of specific protein with Buffer B (50 mM Tris-HCl, pH 8.0, 10 mM reduced glutathione). Fractions (500 μl) containing the GST-tagged CG12004 peptide sequences were confirmed by SDS-PAGE. Purified GST tagged TMEM184B peptides TMEM184B 1–67 and TMEM184B 393–486 in equal proportions (1:1) were injected into rabbits using the Eurogentec Polyclonal Antibody Production service (Eurogentec, Belgium) using an 87 day protocol. To affinity purify anti-Tmep antibodies, 40 μg of each purified peptide were mixed, run on an SDS-PAGE gel and blotted to PVDF. The membrane was blocked with 5% milk and incubated with 1:100 anti-Tmep serum in 1% milk overnight at 4°C. The antibody was eluted using 0.2 M glycine solution, pH 2.3 and neutralized with 1 M Tris base.

Viability Measurement

Tmep^{Cri}/*TM3,Sb* females were crossed to *Df6087/TM6B,TbSb* (non-rescue) or *Df6087, UAS-mKate-Tmep/TM6B,TbSb* (rescue) males. In these crosses, because *TM3/TM6* is viable, we expected 25% of each cross to be non-Sb if the Tmep genotype was fully viable. We compared the resulting percent of non-Sb progeny to the expected for each cross. Vials in which at least 100 progeny emerged over 14 days were included in analysis.

Locomotor Analysis

For crawling assays, wandering third instar larvae were evaluated. Larvae were rinsed quickly in water, dabbed briefly on a kimwipe to remove excess water, and placed on a clear agar dish. The number of full body pericyclic contractions were visually counted over one minute, either in real time or following video recording and analysis. Sample sizes of 20 larvae per sex were used for every condition. Statistics were calculated as described in the Statistical Methods section. For adults: Three-day-old adult flies were minimally anaesthetised with CO_2, placed into 2.0 ml microcentrifuge tubes, and left for 10 min to recover. Flies were then vortexed for 1 min at max speed (Whirlimixer, Fisons Scientific

Apparatus, U.K.). After 1 min recovery, the flies were knocked to bottom of the tube and time taken to reach the top of the tube were measured. A light was placed above the tube to promote phototaxis.

Immunohistochemistry

Larvae were dissected in cold phosphate-buffered saline (PBS), fixed in 4% formaldehyde in PBS, washed with PBST (0.1% Triton X-100), and incubated with primary antibodies overnight at 4°C. Antibodies used include anti-Bruchpilot (Developmental Studies Hybridoma Bank (DSHB), antibody nc82, used at 1:50), anti-HRP (Jackson Immunoresearch, 123-605-021, used at 1:1000), anti-RFP (ThermoFisher # R10367, used at 1:2000), anti-Repo (DSHB, used at 1:20), anti-Synaptotagmin [57], anti-discs-large (DLG) (DSHB, used at 1:2000), anti-Futsch (DSHB antibody 22C10, used at 1:20), and anti-HP1 (DSHB C1A9, used at 1:20). Affinity purified rabbit anti-Tmep was used at 1:20.

Fluorescent Microscopy

For all microscopy experiments actively behaving third instar larvae were used. Image stacks for co-localization analysis were taken on a Zeiss LSM880 inverted confocal microscope in the Marley Light Microscopy Core Facility at the University of Arizona using a 63x/1.4 NA oil objective. The 488, 561, and 633 nm lasers were used to excite GFP, Cy3, and Cy5, respectively. For figure 3d, we used an Elyra 7 structured illumination microscope. Maximum intensity projections or single slices were created as noted in figure legends, exported as TIFs, and analyzed in Fiji (National Institutes of Health).

Colocalization Analysis

Confocal pictures (Zeiss LSM 880) were used for analysis, and all larvae were imaged with identical settings. All subsequent analysis was done in Fiji. Images were imported into Fiji using the BioFormats plugin. To quantify colocalization, we first separated channels. For each channel, a uniform threshold was chosen based on an appropriate (by eye) capture of all positive pixels in a wild type larva. This threshold was applied for all images from both wild type and mutant larvae. These thresholded images were binarized, and the Manders' Correlation Coefficient was calculated from the binary images. This analysis discards intensity information for each puncta, allowing the overall number of overlapping pixels to be calculated using Manders' Correlation Coefficient. For Rab11, 66 neuronal cell bodies over 3 larvae were analyzed. For nSyb, 2 synapses (onto either muscle 6/7 or muscle 4) per larvae over 3 larvae were analyzed.

Calcium Imaging and Analysis

Female third instar larvae of the desired genotype were dissected in a small volume of ice-cold HL3.1 [58] with 0.1 mM Ca^{2+} using pins in a shallow Sylgard-coated dish (3.5 cm). Following removal of guts, solution was exchanged twice, removed, and replaced by 200 µl of cold HL3.1 with 0.5 mM Ca^{2+} for imaging. All solutions contained 7 mM glutamate to desensitize glutamate receptors on muscles, enabling less muscle contraction during analysis [59]. The dish was directly mounted onto the stage of a Zeiss LSM880 NLO upright multiphoton/confocal microscope with a 40x water-immersion objective. Laser lines

488 and 561 nm were used to excite GcaMP5G and tdTomato, respectively. We were able to obtain baseline calcium images at 10 minutes following the start of dissection, as this was the fastest that the prep could be dissected, washed, mounted, and a synapse could be identified for imaging. To find a synapse, we used brightfield to locate healthy muscles where nerves appeared to be attached. Scanning to find synapses was hastened as much as possible due to bleaching effects on fluorophores. Images were taken at 1024 × 1024 resolution. Within a channel, all images were taken at the same laser gain and intensity.

For ratiometric analysis, we recorded a pipeline in Fiji and used it for all images. Individual channels were first background subtracted (rolling ball, radius 100) and converted to 8-bit. The TdTomato signal was thresholded (minimum 40) and binarized, and a mask image was created. By applying the mask to both the TdTomato and GcaMP5G images, only pixels within axons and synapses were retained. Regions of interest (boutons) were manually drawn around the TdTomato-filled boutons. Measurements of area and integrated density were exported to text files and processed using a custom script in R. Briefly, for each channel, the sum of bouton areas and the sum of raw integrated densities was calculated. The normalized integrated density was calculated for each channel by dividing the raw ID by the area. Then the green/red ratio was calculated for each synapse as a whole. Synapses from 5–6 larvae were evaluated per genotype. Statistical comparison was done in Graphpad Prism using unpaired t-test.

Synapse morphology analysis

Synapse morphology analysis was carried out at muscles 6/7, hemisegment A3. Boutons were defined as distinct, spherical, anti-synaptotagmin–positive varicosities contacting the muscle. Measurements were made from images using Fiji. For branching analysis, Fiji plugin NeuronJ was used (https://imagej.net/plugins/neuronj). The extent of branching was estimated by dividing synapse length by the number of branches, where a branch was defined as any section from the synapse core which was longer than 10 μm.

Bouton and Active Zone Quantification

To analyze active zones, image stacks were taken using an LSM 880 Confocal with AiryScan mode and processed using the 3D setting. Active zone density was determined by manually calculating Brp positive spots per bouton area (determined by positive synaptotagmin staining). Bouton area was calculated using the Measure function in Fiji. Total of 6 synaptic terminals of different animals were analyzed per genotype, each synaptic terminal containing 5–7 boutons.

Satellite boutons were defined according to previous work [60–62] as small laterally branched boutons emerging from a primary axis with three or less smaller bouton sprouts. We imaged boutons using a ZEISS Elyra 7 with Lattice SIM^2 confocal. Images were taken with 13 phases and processed using a “weak processing” setting. Quantification was performed by dividing the number of satellite boutons by synapse branch length. N = 5 larvae per genotype; statistical comparison used unpaired t-test.

Electrophysiology

Larvae were fillet dissected in ice-cold HL 3.1 with 0.1 mM calcium, and then washed into 0.4 mM calcium HL 3.1. We performed recordings of muscle 6, abdominal segment 3. A single recording was collected per larvae to minimize dissected time and maximize the health of our preparations. All electrodes were pulled using a flaming/brown micropipette puller (Sutter Instruments Model P-97). We used stimulating electrodes from Drummond (#1-000-0500), which we melted to 2–3 mm in diameter using a heated filament (Narishige Microforge, MF-830). Recording electrodes (WPI (#TW150F-3) were filled with 3M KCl and were typically 20–40 MOhms in resistance. To be included in analysis, baseline muscle potential needed to be between −55 and −72 mV, and baseline could not deviate more than 10 mV within this range during the entire recording. Once stabilized in this range, we recorded spontaneous mEJPs for 15–30 seconds. Axons were then stimulated (3.3 mV, 0.1 ms, 0.2 Hz) at least 10 times (A-M Systems isolated pulse stimulator, model 2100). Voltage signals were amplified with an Axoclamp 2B amplfiier (Axon Instruments) and digitized with a DigiData 1200 interface and pClamp 10.0 software (Axon Instruments). For EJPs, four larvae per genotype and at least 10 post-stimulus responses were analyzed. Once chosen, baselines were manually adjusted to fit a straight line using Clampfit (versions 10.7 and 11.2). Using the threshold search function, we set a low threshold for detection of mEJP (0.2 mV) and EJP (5 mV) and manually excluded those signals that were above threshold but were not appropriately called. This enabled the inclusion and quantification of small multi-EJP events in mutant larvae. EJP amplitudes, mEJP amplitudes, and inter-event intervals were exported from Clampfit into a CSV file and analyzed using Graphpad Prism.

Transmission Electron Microscopy

Third instar wandering larvae were dissected and fixed in 0.1M $NaPO_4$ (pH 7.4), 1% gluteraldehyde and 4 % formaldehyde (pH 7.3) overnight. Fixed larval preparations were washed 3x in 0.1 M $NaPO_4$ prior to incubation in OsO_4 (1% in 0.1 M $NaPO_4$, 2 hr). Preparations were washed 3x in dH_2O before incubation in 1% uranyl acetate. Preparations were washed (3x dH_2O) and dehydrated through a graded ethanol series; 20 % increments starting at 30 % followed by two 100 % changes, then 2× 100% propylene oxide. Preps were incubated in a graded series of Epon araldite resin (in propylene oxide); 25% increments culminating in 3× 100 % changes. Individual muscles and the ventral nerve cord were then dissected out. These were then transferred into embedding molds and the resin polymerized at 60°C for 48 hours. Resin mounted preps were sectioned (60 – 70 nm) using glass knives upon a Leica Ultracut UCT microtome and placed onto grids. Preps were subsequently incubated in uranyl acetate (50% in ethanol), washed in dH_2O and incubated in lead citrate. Sections were imaged using a TECNAI 12 G^2 transmission electron microscope with an SIS Megaview camera and Tecnai user interface v2.1.8 and analySIS v3.2.

Statistical Processing

All statistical comparisons were evaluated using GraphPad Prism (version 9.2.0). In all analyses, only within-sex comparisons were performed due to our observation of sexually dimorphic phenotypes. For viability, we used one-way ANOVA followed by Sidak's multiple comparisons correction. For locomotor analysis of larvae, we performed 2-way

ANOVA using Bonferroni's multiple comparisons test. Unless otherwise specified, animals were only compared within sex using two-tailed T-tests.

Acknowledgements.

The authors would like to thank all members of the Bhattacharya lab for thoughtful comments on the manuscript. We also thank Dr. Konrad Zinsmaier for sharing his electrophysiology equipment as well as his expertise for our work. We thank Drs. Kimberly Chapman and Seth Berger at Children's National Medical Center for communicating unpublished information. We thank the York Protein Production Facility, the York Imaging and Cytometry Facility, and the University of Arizona Marley Microscopy Core Facility for their assistance.

Funding

This work was supported by R01NS105680, a Muscular Dystrophy Association Development grant, and the Arizona Technology and Research Initiative Fund (TRIF) (to M.R.C.B.), the MRC (UK) grant MR/M013596/1 to S.T.S. and a Biotechnology and Biological Sciences Research Council Studentship grant BB/M011151/1 (to S.T.S. and E.B.).

Data and Materials Availability

Flies and plasmids created during this study will be available from the authors or deposited at the Bloomington Drosophila Stock Center (BDSC) or at Addgene.

References

1. Schneggenburger R, Neher E (2005) Presynaptic calcium and control of vesicle fusion. Curr. Opin. Neurobiol 15:266–274 [PubMed: 15919191]
2. Kwon SK, Sando R, Lewis TL, et al. (2016) LKB1 Regulates Mitochondria-Dependent Presynaptic Calcium Clearance and Neurotransmitter Release Properties at Excitatory Synapses along Cortical Axons. PLoS Biol 14:. 10.1371/journal.pbio.1002516
3. Brusich DJ, Spring AM, James TD, et al. (2018) Drosophila CaV2 channels harboring human migraine mutations cause synapse hyperexcitability that can be suppressed by inhibition of a Ca2+store release pathway. PLoS Genet 14:. 10.1371/journal.pgen.1007577
4. Stern M, Ganetzky B (1989) Altered synaptic transmission in drosophila hyperkinetic mutants. J Neurogenet 5:215–228. 10.3109/01677068909066209 [PubMed: 2553904]
5. Uytterhoeven V, Kuenen S, Kasprowicz J, et al. (2011) Loss of Skywalker reveals synaptic endosomes as sorting stations for synaptic vesicle proteins. Cell 145:117–132. 10.1016/j.cell.2011.02.039 [PubMed: 21458671]
6. Fernandes AC, Uytterhoeven V, Kuenen S, et al. (2014) Reduced synaptic vesicle protein degradation at lysosomes curbs TBC1D24/sky-induced neurodegeneration. J Cell Biol 207:453–462. 10.1083/JCB.201406026 [PubMed: 25422373]
7. Fischer B, Lüthy K, Paesmans J, et al. (2016) Skywalker-TBC1D24 has a lipid-binding pocket mutated in epilepsy and required for synaptic function. Nat Struct Mol Biol 23:965–973. 10.1038/nsmb.3297 [PubMed: 27669036]
8. Koh TW, Korolchuk VI, Wairkar YP, et al. (2007) Eps15 and Dap160 control synaptic vesicle membrane retrieval and synapse development. J Cell Biol 178:309–322. 10.1083/jcb.200701030 [PubMed: 17620409]
9. Milton VJ, Jarrett HE, Gowers K, et al. (2011) Oxidative stress induces overgrowth of the Drosophila neuromuscular junction. Proc Natl Acad Sci U S A 108:17521–17526. 10.1073/pnas.1014511108 [PubMed: 21987827]
10. West RJH, Briggs L, Fjeldstad MP, et al. (2018) Sphingolipids regulate neuromuscular synapse structure and function in Drosophila. J Comp Neurol 526:1995. 10.1002/CNE.24466 [PubMed: 29761896]

11. Hindle SJ, Hebbar S, Schwudke D, et al. (2017) A saposin deficiency model in Drosophila: Lysosomal storage, progressive neurodegeneration and sensory physiological decline. Neurobiol Dis 98:77–87. 10.1016/j.nbd.2016.11.012 [PubMed: 27913291]
12. Vivas O, Tiscione SA, Dixon RE, et al. (2019) Niemann-Pick Type C Disease Reveals a Link between Lysosomal Cholesterol and PtdIns(4,5)P2 That Regulates Neuronal Excitability. Cell Rep 27:2636. 10.1016/J.CELREP.2019.04.099 [PubMed: 31141688]
13. Wucherpfennig T, Wilsch-Bräuninger M, González-Gaitán M (2003) Role of Drosophila Rab5 during endosomal trafficking at the synapse and evoked neurotransmitter release. J Cell Biol 161:609–624. 10.1083/jcb.200211087 [PubMed: 12743108]
14. Ackermann F, Schink KO, Bruns C, et al. (2019) Critical role for piccolo in synaptic vesicle retrieval. Elife 8:. 10.7554/eLife.46629
15. Vazquez-Sanchez S, Gonzalez-Lozano MA, Walfenzao A, et al. (2020) The endosomal protein sorting nexin 4 is a synaptic protein. Sci Rep 10:. 10.1038/s41598-020-74694-6
16. Li YC, Kavalali ET (2017) Synaptic vesicle-recycling machinery components as potential therapeutic targets. Pharmacol. Rev 69:141–160 [PubMed: 28265000]
17. Bhattacharya MRC, Geisler S, Pittman SK, et al. (2016) TMEM184b promotes axon degeneration and neuromuscular junction maintenance. J Neurosci 36:4681–4689. 10.1523/JNEUROSCI.2893-15.2016 [PubMed: 27122027]
18. Larsen EG, Cho TS, McBride ML, et al. TMEM184B is necessary for IL-31-induced itch. PAIN (in Press. 10.1101/2020.01.25.919902
19. Lee PT, Zirin J, Kanca O, et al. (2018) A gene-specific T2A-GAL4 library for drosophila. Elife 7:4. 10.7554/eLife.35574
20. Haberman A, Williamson WR, Epstein D, et al. (2012) The synaptic vesicle SNARE neuronal synaptobrevin promotes endolysosomal degradation and prevents neurodegeneration. J Cell Biol 196:261–276. 10.1083/jcb.201108088 [PubMed: 22270918]
21. Dickman DK, Lu Z, Meinertzhagen IA, Schwarz TL (2006) Altered synaptic development and active zone spacing in endocytosis mutants. Curr Biol 16:591–598. 10.1016/J.CUB.2006.02.058 [PubMed: 16546084]
22. Burg MG, Wu C-F (2012) Mechanical and temperature stressors-induced seizure-and-paralysis behaviors in Drosophila bang-sensitive mutants. J Neurogenet 26:189. 10.3109/01677063.2012.690011 [PubMed: 22716921]
23. Daniels RW, Rossano AJ, Macleod GT, Ganetzky B (2014) Expression of Multiple Transgenes from a Single Construct Using Viral 2A Peptides in Drosophila. PLoS One 9:e100637. 10.1371/JOURNAL.PONE.0100637 [PubMed: 24945148]
24. Simkus CRL, Stricker C (2002) The contribution of intracellular calcium stores to mEPSCs recorded in layer II neurones of rat barrel cortex. J Physiol 545:521–535. 10.1113/JPHYSIOL.2002.022103 [PubMed: 12456831]
25. Wong CO, Chen K, Lin YQ, et al. (2014) A TRPV channel in drosophila motor neurons regulates presynaptic resting Ca2+ levels, synapse growth, and synaptic transmission. Neuron 84:764–777. 10.1016/j.neuron.2014.09.030 [PubMed: 25451193]
26. de Juan-Sanz J, Holt GT, Schreiter ER, et al. (2017) Axonal Endoplasmic Reticulum Ca2+ Content Controls Release Probability in CNS Nerve Terminals. Neuron 93:867–881.e6. 10.1016/j.neuron.2017.01.010 [PubMed: 28162809]
27. Bezprozvanny I, Kavalali ET (2020) Presynaptic endoplasmic reticulum and neurotransmission. Cell Calcium 85:102133. 10.1016/J.CECA.2019.102133 [PubMed: 31812114]
28. Chanaday NL, Nosyreva E, Shin OH, et al. (2021) Presynaptic store-operated Ca2+ entry drives excitatory spontaneous neurotransmission and augments endoplasmic reticulum stress. Neuron 109:1314–1332.e5. 10.1016/J.NEURON.2021.02.023 [PubMed: 33711258]
29. Russo A, Goel P, Brace E, et al. (2019) The E3 ligase Highwire promotes synaptic transmission by targeting the NAD-synthesizing enzyme dNmnat. EMBO Rep 20:e46975. 10.15252/EMBR.201846975 [PubMed: 30692130]
30. Mack TGA, Reiner M, Beirowski B, et al. (2001) Wallerian degeneration of injured axons and synapses is delayed by a Ube4b/Nmnat chimeric gene. Nat Neurosci 4:1199–1206. 10.1038/nn770

31. Sasaki Y, Vohra BPS, Baloh RH, Milbrandt J (2009) Transgenic mice expressing the nmnatl protein manifest robust delay in axonal degeneration in vivo. J Neurosci 29:6526–6534. 10.1523/JNEUROSCI.1429-09.2009 [PubMed: 19458223]
32. Sasaki Y, Milbrandt J (2010) Axonal degeneration is blocked by nicotinamide mononucleotide adenylyltransferase (Nmnat) protein transduction into transected axons. J Biol Chem 285:41211–41215. 10.1074/JBC.C110.193904 [PubMed: 21071441]
33. Fritschy JM (2008) Epilepsy, E/I balance and GABAA receptor plasticity. Front Mol Neurosci 1:. 10.3389/neuro.02.005.2008
34. Bozzi Y, Provenzano G, Casarosa S (2018) Neurobiological bases of autism–epilepsy comorbidity: a focus on excitation/inhibition imbalance. Eur J Neurosci 47:534–548. 10.1111/ejn.13595 [PubMed: 28452083]
35. Liu XM, Yamasaki A, Du XM, et al. (2018) Lipidation-independent vacuolar functions of atg8 rely on its noncanonical interaction with a vacuole membrane protein. Elife 7:1–21. 10.7554/eLife.41237
36. He CW, Cui XF, Ma SJ, et al. (2021) Membrane recruitment of Atg8 by Hfl1 facilitates turnover of vacuolar membrane proteins in yeast cells approaching stationary phase. BMC Biol 19:. 10.1186/s12915-021-01048-7
37. Liu Q, Vain T, Viotti C, et al. (2018) Vacuole Integrity Maintained by DUF300 Proteins Is Required for Brassinosteroid Signaling Regulation. Mol Plant 11:553–567. 10.1016/j.molp.2017.12.015 [PubMed: 29288738]
38. Kittel RJ, Wichmann C, Rasse TM, et al. (2006) Bruchpilot promotes active zone assembly, Ca2+ channel clustering, and vesicle release. Science 312:1051–1054. 10.1126/SCIENCE.1126308 [PubMed: 16614170]
39. Wagh DA, Rasse TM, Asan E, et al. (2006) Bruchpilot, a Protein with Homology to ELKS/CAST, Is Required for Structural Integrity and Function of Synaptic Active Zones in Drosophila. Neuron 49:833–844. 10.1016/J.NEURON.2006.02.008 [PubMed: 16543132]
40. Shakiryanova D, Morimoto T, Zhou C, et al. (2011) Differential Control of Presynaptic CaMKII Activation and Translocation to Active Zones. J Neurosci 31:9093. 10.1523/JNEUROSCI.0550-11.2011 [PubMed: 21697360]
41. Narita K, Akita T, Osanai M, et al. (1998) A Ca2+-induced Ca2+ release mechanism involved in asynchronous exocytosis at frog motor nerve terminals. J Gen Physiol 112:593–609. 10.1085/JGP.112.5.593 [PubMed: 9806968]
42. Kubota M, Narita K, Murayama T, et al. (2005) Type-3 ryanodine receptor involved in Ca2+-induced Ca2+ release and transmitter exocytosis at frog motor nerve terminals. Cell Calcium 38:557–567. 10.1016/j.ceca.2005.07.008 [PubMed: 16157373]
43. Khuzakhmetova V, Samigullin D, Nurullin L, et al. (2014) Kinetics of neurotransmitter release in neuromuscular synapses of newborn and adult rats. Int J Dev Neurosci 34:9–18. 10.1016/J.IJDEVNEU.2013.12.010 [PubMed: 24412779]
44. Khuzakhmetova VF, Samigullin DV, Bukharaeva EA (2014) The role of presynaptic ryanodine receptors in regulation of the kinetics of the acetylcholine quantal release in the mouse neuromuscular junction. Biochem Suppl Ser A Membr Cell Biol 2014 81 8:144–152. 10.1134/S199074781305005X
45. James TD, Zwiefelhofer DJ, Frank CA (2019) Maintenance of homeostatic plasticity at the Drosophila neuromuscular synapse requires continuous IP 3-directed signaling. Elife 8:. 10.7554/ELIFE.39643
46. Kaeser PS, Regehr WG (2014) Molecular Mechanisms for Synchronous, Asynchronous, and Spontaneous Neurotransmitter Release. http://dx.doi.org/101146/annurev-physiol-021113-170338 76:333–363. 10.1146/ANNUREV-PHYSIOL-021113-170338
47. Budnik V, Zhong Y, Wu CF (1990) Morphological plasticity of motor axons in Drosophila mutants with altered excitability. J Neurosci 10:3754–3768. 10.1523/JNEUROSCI.10-11-03754.1990 [PubMed: 1700086]
48. Kuebler D, Zhang H, Ren X, Tanouye MA (2001) Genetic suppression of seizure susceptibility in Drosophila. J Neurophysiol 86:1211–1225. 10.1152/JN.2001.86.3.1211/ASSET/IMAGES/LARGE/9K0911880007.JPEG [PubMed: 11535671]

49. Saras A, Tanouye MA (2016) Mutations of the Calcium Channel Gene cacophony Suppress Seizures in Drosophila. PLOS Genet 12:e1005784. 10.1371/JOURNAL.PGEN.1005784 [PubMed: 26771829]
50. Wiel C, Lallet-Daher H, Gitenay D, et al. (2014) Endoplasmic reticulum calcium release through ITPR2 channels leads to mitochondrial calcium accumulation and senescence. Nat Commun 5:. 10.1038/ncomms4792
51. Wong CO, Karagas NE, Jung J, et al. (2021) Regulation of longevity by depolarization-induced activation of PLC-β-IP3R signaling in neurons. Proc Natl Acad Sci U S A 118:1–9. 10.1073/pnas.2004253118
52. Calcraft PJ, Ruas M, Pan Z, et al. (2009) NAADP mobilizes calcium from acidic organelles through two-pore channels. Nature 459:596–600. 10.1038/NATURE08030 [PubMed: 19387438]
53. Meyer JO, Dolphin AC (2021) Rab11-dependent recycling of calcium channels is mediated by auxiliary subunit α2δ−1 but not α2δ−3. Sci Rep 11:1–13. 10.1038/s41598-021-89820-1 [PubMed: 33414495]
54. Malek M, Wawrzyniak AM, Koch P, et al. (2021) Inositol triphosphate-triggered calcium release blocks lipid exchange at endoplasmic reticulum-Golgi contact sites. Nat Commun 12:. 10.1038/s41467-021-22882-x
55. Saheki Y, De Camilli P (2017) Endoplasmic Reticulum–Plasma Membrane Contact Sites. Annu Rev Biochem 86:659–684. 10.1146/annurev-biochem-061516-044932 [PubMed: 28301744]
56. Davis GW, Schuster CM, Goodman CS (1997) Genetic Analysis of the Mechanisms Controlling Target Selection: Target-Derived Fasciclin II Regulates the Pattern of Synapse Formation. Neuron 19:561–573. 10.1016/S0896-6273(00)80372-4 [PubMed: 9331349]
57. West RJH, Lu Y, Marie B, et al. (2015) Rab8, POSH, and TAK1 regulate synaptic growth in a Drosophila model of frontotemporal dementia. J Cell Biol 208:931–947. 10.1083/jcb.201404066 [PubMed: 25800055]
58. Feng Y, Ueda A, Wu CF (2004) A modified minimal hemolymph-like solution, HL3.1, for physiological recordings at the neuromuscular junctions of normal and mutant Drosophila larvae. J Neurogenet 18:377–402. 10.1080/01677060490894522 [PubMed: 15763995]
59. Macleod GT, Marin L, Charlton MP, Atwood HL (2004) Synaptic Vesicles: Test for a Role in Presynaptic Calcium Regulation. J Neurosci 24:2496–2505. 10.1523/JNEUROSCI.5372-03.2004 [PubMed: 15014125]
60. Marie B, Sweeney ST, Poskanzer KE, et al. (2004) Dap160/Intersectin scaffolds the periactive zone to achieve high-fidelity endocytosis and normal synaptic growth. Neuron 43:207–219. 10.1016/j.neuron.2004.07.001 [PubMed: 15260957]
61. Beumer KJ, Rohrbough J, Prokop A, Broadie K (1999) A role for PS integrins in morphological growth and synaptic function at the postembryonic neuromuscular junction of Drosophila. Development 126:5833–5846. 10.1242/dev.126.24.5833 [PubMed: 10572057]
62. Torroja L, Packard M, Gorczyca M, et al. (1999) The Drosophila β-amyloid precursor protein homolog promotes synapse differentiation at the neuromuscular junction. J Neurosci 19:7793–7803. 10.1523/jneurosci.19-18-07793.1999 [PubMed: 10479682]

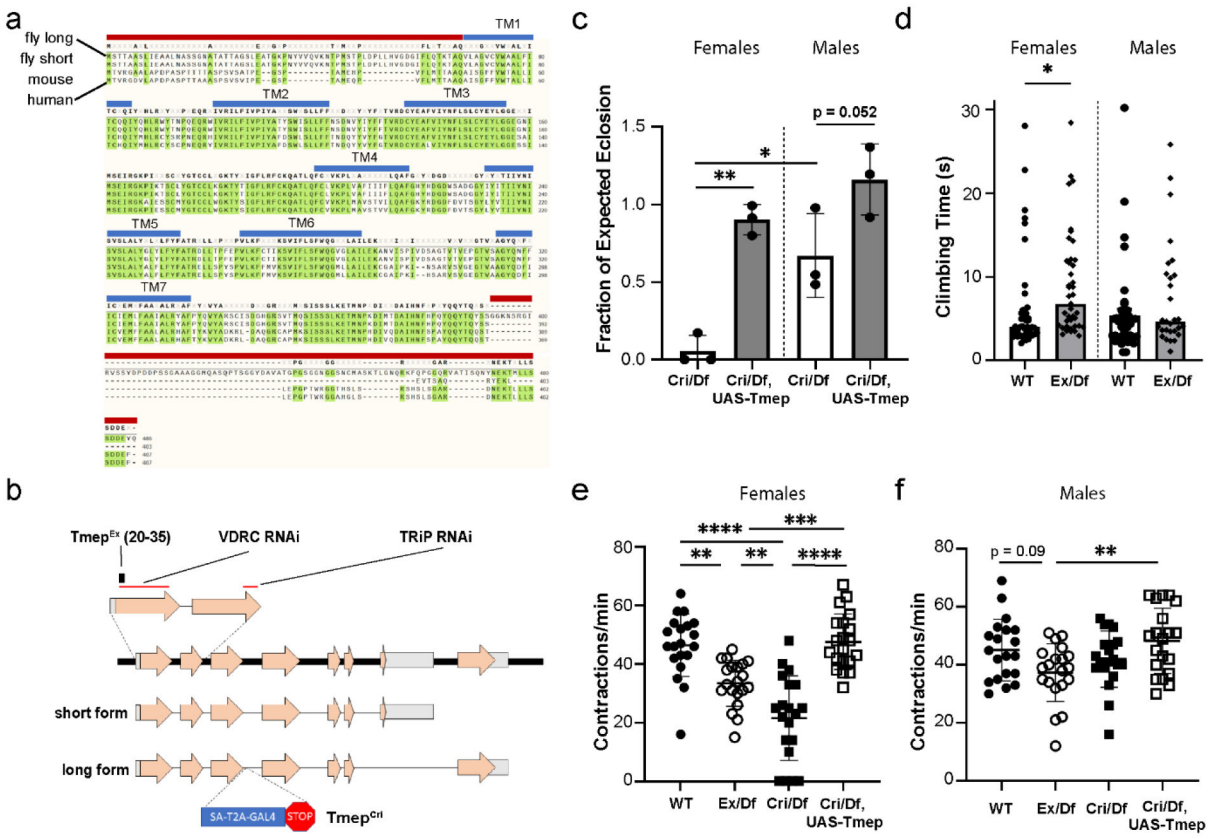

Figure 1. CG12004 (Tmep), a *Drosophila* protein with high homology to mammalian TMEM184b, is needed for full viability and locomotor function.

a, Alignment of *Drosophila*, mouse, and human TMEM184B proteins. Top to bottom: CG12004 long isoform, CG12004 short isoform, mouse TMEM184b isoform, human TMEM184b isoform. Transmembrane segments (blue lines) and sequences used for antibody generation (red lines) are shown. **b**, Schematic drawing of the CG12004 genomic region on Chromosome 3. Mutations and regions targeted by knockdown constructs used in this study are indicated. **c**, Rates of eclosion of $Tmep^{Cri}$/Df (*Cri/Df*) in both sexes and rescue by UAS-Tmep (N-terminal mKate-tagged). P values: Male vs Female $Tmep^{Cri}/Df$, p = 0.016; Male $Tmep^{Cri}/Df$ vs Rescue, p = 0.052; Female $Tmep^{Cri}$/Df vs Rescue, p = 0.0024. N = 3 independent crosses with 5 male and 5 female parents in each cross. Statistical evaluation was done using one-way ANOVA with Sidak's multiple comparisons test. **d**, climbing assay after disorientation of wild type and $Tmep^{Ex}/Df$ (*Ex/Df*) females and males. N = 43, 41, 42, 29 flies (left to right). For females, p = 0.045, unpaired t-test. **e-f**, larval contraction rate by genotype and sex (e shows females, f shows males). P values for females: wild type vs $Tmep^{Ex}/Df$, p = 0.0017; wild type vs $Tmep^{Cri}$/Df, p < 0.0001; $Tmep^{Ex}/Df$ vs $Tmep^{Cri}/Df$, p = 0.005; $Tmep^{Ex}/Df$ vs rescue, p = 0.0005; $Tmep^{Cri}/Df$ vs Rescue, p < 0.0001; wild type vs rescue, p = 0.98. For males, all comparisons were p > 0.05 except $Tmep^{Ex}/Df$ vs rescue, where p = 0.008. N = 20 for all genotypes. Statistical significance was calculated by one-way ANOVA with Bonferroni's multiple comparison correction.

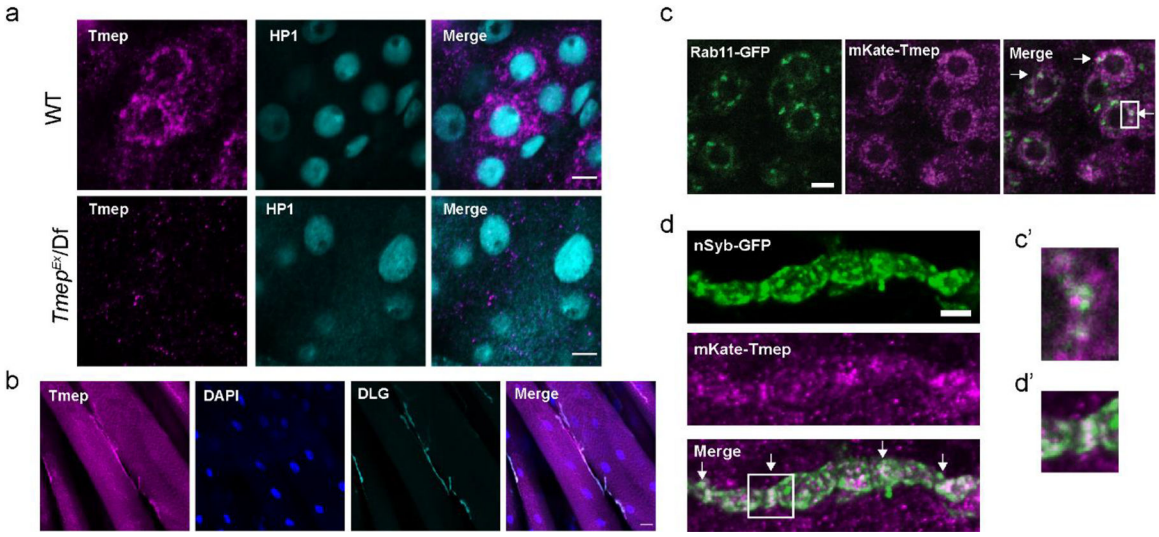

Figure 2. Tmep localizes to neuronal endosomes and synaptic vesicles.

a, Antibody to *Drosophila* Tmep shows neuronal staining in the larval ventral nerve cord. Magenta, Tmep; Teal, HP1 (nuclei). Image is from the area where motor neurons reside. Limited staining is observed in Tmep mutants (*$Tmep^{Ex}$/Df*). Scale bar = 5 μm. **b**, Tmep protein levels at the neuromuscular junction. Magenta, Tmep; Blue, DAPI; Teal, *discs large* (DLG) showing the postsynaptic area. Scale bar = 20 μm. **c,** Tmep shows partial colocalization with Rab11-positive endosomes. Motor neuron expression of mKate-Tmep (magenta) and Rab11-GFP (green) is driven by *BG380-GAL4*. Image is a single confocal slice of cell bodies in the ventral neve cord; arrows in the merged image show areas of partial colocalization. Scale bar = 5 μm. **c',** expanded view of the boxed region in c. **d**, Tmep shows partial colocalization with synaptic vesicles at the larval NMJ. Image is a single confocal slice. Nsyb-GFP and mKate were expressed as in c. Scale bar = 5 μm. **d',** expanded view of the boxed region in d.

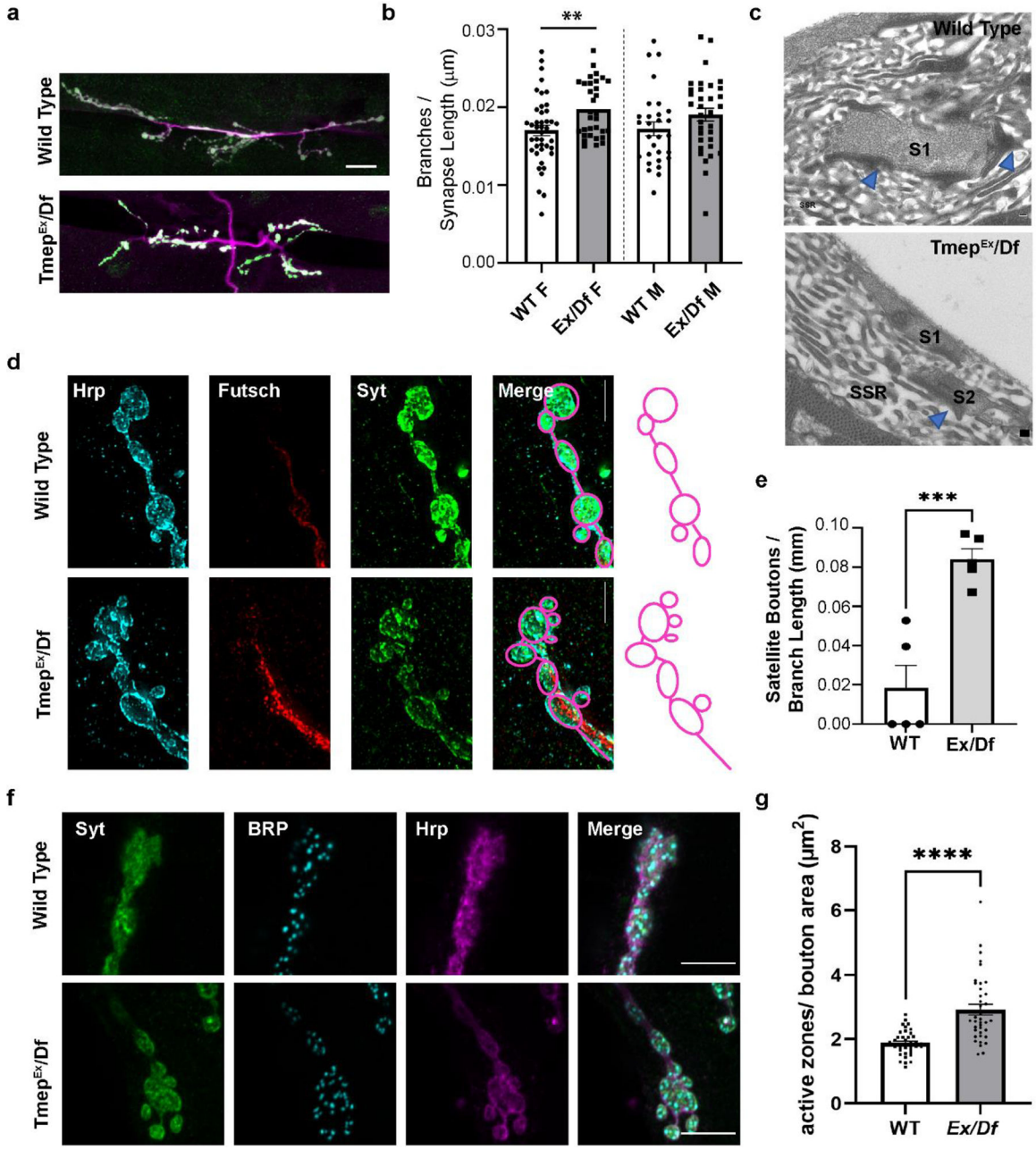

Figure 3. Tmep mutant larvae show extra branches, boutons, and active zones at the neuromuscular junction.

All images show wandering female third instar larvae. **a**, Representative images of muscle 6/7 NMJs stained with antibodies to Synaptotagmin (Syt, green) and HRP (magenta) illustrating branching phenotypes. Scale bar = 20 μm. **b**, Quantification of branches in wild type or *Ex/Df* larvae. Branch count is normalized to the total synapse length (sum of all branches). **c**, Representative transmission EM sections of segment A3, muscle 6/7 from 3rd instar larvae. Blue arrows indicate presynaptic dense bodies (T-bars). Synapses (electron-dense areas) are labelled by S (S1, S2). Subsynaptic reticulum area is marked as SSR. Ex/Df synapse shows two boutons' sections in the same plane, suggesting possible

bouton fragmentation at the synaptic terminal. Scale bar = 200 nm. **d**, Synaptic terminal boutons in wild type and *Ex/Df* showing an example of satellite boutons at the mutant NMJ. HRP (blue), Futsch (red), and Synaptotagmin (Syt, green) are shown. Scale bar = 5 μm. Drawings illustrate the bouton structure in the images. **e**, Satellite bouton quantification normalized to the length of the branch upon which the boutons are located. N = 5 female larvae per genotype. p = 0.0009 using unpaired t-test. **f**, representative images showing active zone density at presynaptic terminal boutons. Syt (green), Bruchpilot (BRP, light blue) and HRP (magenta) are shown. **g**, quantification of active zone density per square micron of bouton area in female larvae. N = 6 animals, n= 38 total boutons analyzed per genotype. Statistical comparison used unpaired t-test ($p < 0.0001$).

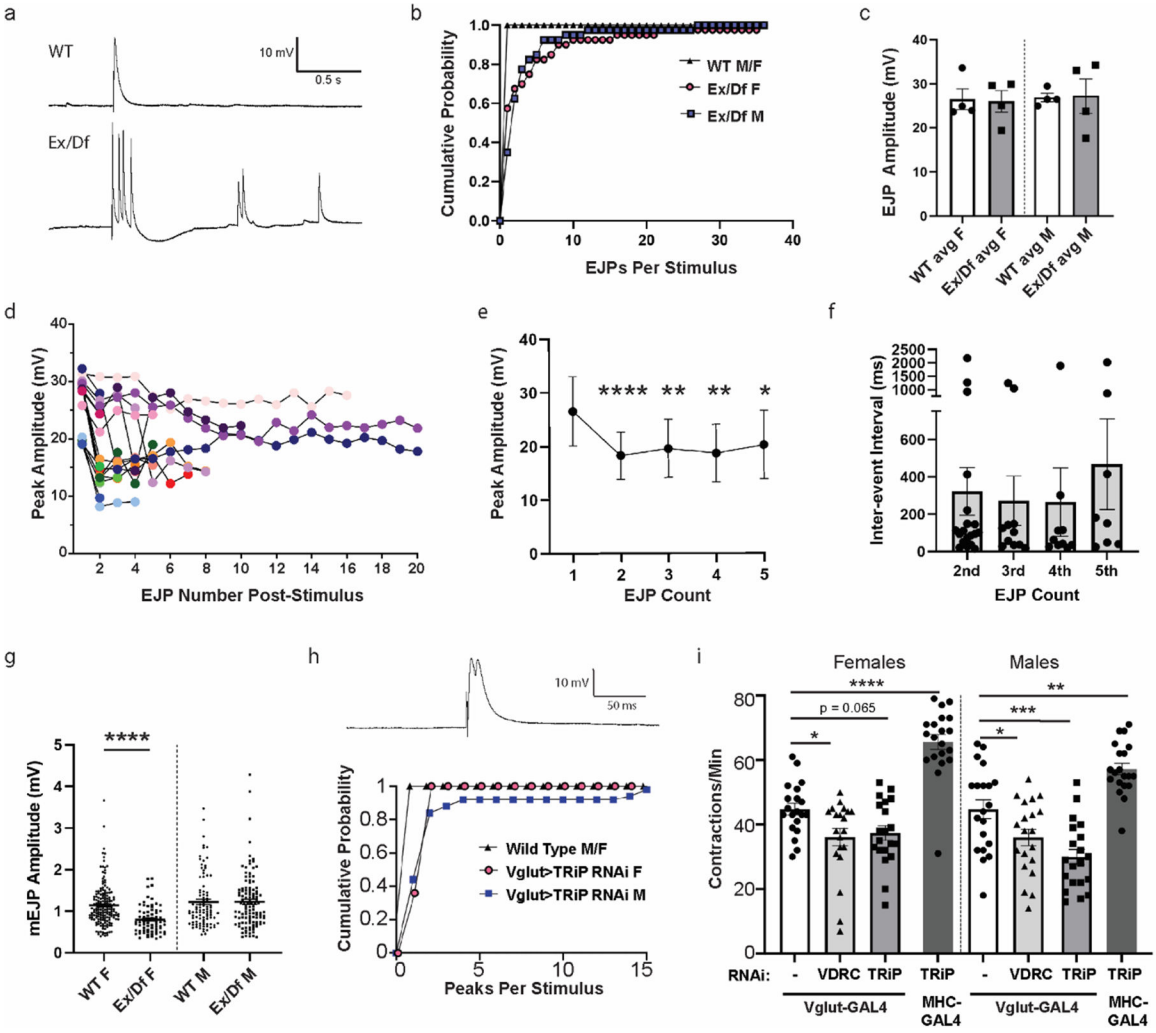

Figure 4. Tmep is required for proper synaptic transmission.

a, Representative examples of evoked junctional potentials (EJPs) evoked by stimulation of wild type (WT) or *Tmep*^{Ex}/*Df* (*Ex/Df*) female neuromuscular junctions (1 ms, 3.3 mV). **b-e**, Analysis of EJPs from N=4 larvae/genotype and n=10 stimuli/larvae. **b**, Cumulative probability of single and multiple EJPs following stimulation in wild type and *Ex/Df* larvae (over the 5 sec post-stimulation), separated by sex. All recordings were done in 0.4 mM Ca^{2+} HL3.1. **c**, EJP amplitudes of the first response recorded following each stimulus. **d**, Peak amplitudes of EJPs per stimulus. 17 of 40 EJPs measured in 4 *Ex/Df* females showed multiple peaks and are displayed on the graph. **e**, Relative sizes of multi-EJP responses to a single stimulus from female *Ex/Df* larvae. N=17, 17, 13, 12, and 10 stimuli showed at least 5 responses and were included in analysis. Differences from the first peak's amplitude were analyzed by fitting a mixed model using paired comparisons (responses in each larvae), with Dunnett's correction for multiple comparisons. P values: 1st-2nd, p <0.0001; 1st-3rd, p = 0.0072; 1st-4th, p = 0.0016; 1st-5th, p = 0.0336. **f**, Inter-event interval from females shown in e. Only the first five inter-event intervals were analyzed, and each point represents the interval from the previous spike (i.e. 2nd is from spike 1 to spike 2). No significant differences were observed (p > 0.05, one-way ANOVA). **g**, mEJP

amplitudes from wild type and *Ex/Df* larvae of each sex. N=4 larvae per group. Fifteen seconds of baseline recording were analyzed per animal. T-tests within each sex were used to evaluate statistical significance (females, p <0.0001; males, p = 0.98). **h**, representative trace (above) and cumulative probability (below) of multi-peak events in Tmep knockdown (TRiP) larvae using *Vglut-GAL4*. Note that controls (black triangles) do not show any multi-peak responses. N=5 larvae and 10 stimuli/larvae per genotype. **i,** Crawling analysis of larvae in which Tmep is knocked down in motor neurons (*Vglut-GAL4*) or muscle (*MHC-GAL4*) with one of two different RNAi constructs (sequence targets are shown in Figure 1). N=20 animals per genotype and sex. One-way ANOVA with Dunnett's post-hoc test within sex; p = 0.025 (Vglut F alone vs VDRC F), p = 0.065 (Vglut F alone vs TRiP F), p = <0.0001 (Vglut F alone vs MHC> TRiP F), p = 0.035 (Vglut M alone vs TRiP M), p = 0.0002 (Vglut M alone vs TRiP M), p = 0.0016 (Vglut M alone vs MHC> TRiP).

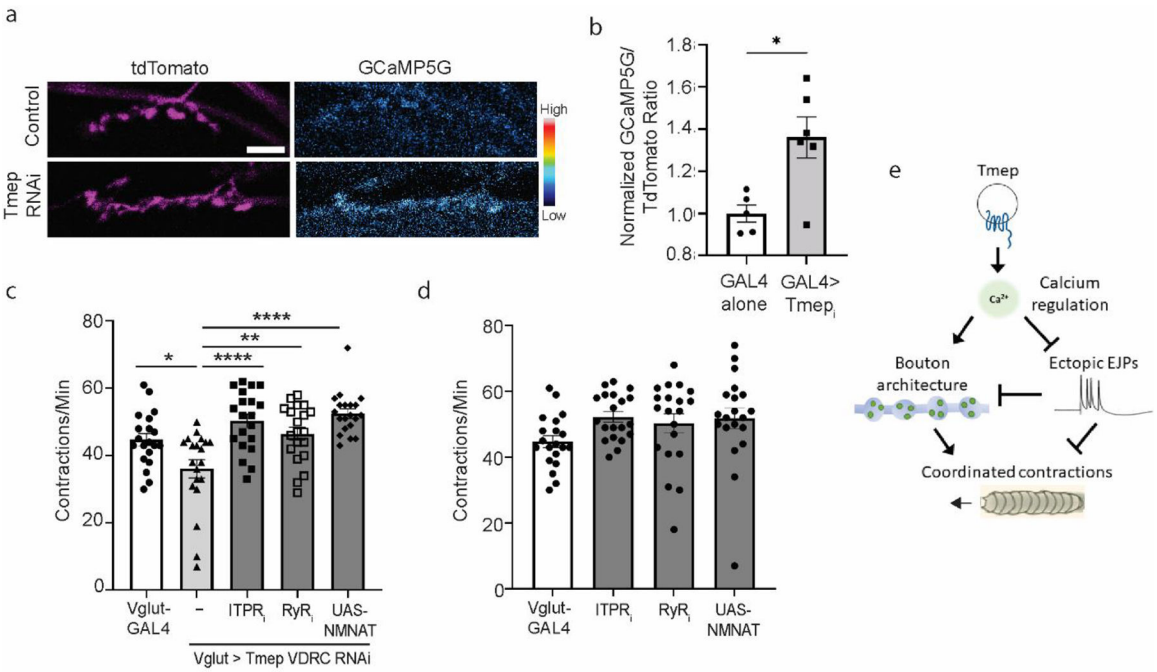

Figure 5. Larval crawling deficiencies are restored by reduction of presynaptic excitability.

a, Representative images of baseline calcium in GAL4 alone (UAS-Dicer2, Vglut-GAL4, UAS-GCaMP5G-T2A-tdTomato) and Tmep RNAi larvae (UAS-Dicer2, Vglut-GAL4, UAS-Tmepi (VDRC), UAS-GcaMP5G-T2A-tdTomato). TdTomato images are pseudocolored with a Magenta look-up table, and GCaMP is pseudocolored with the Cyan Hot lookup table (Fiji), for which the scale is shown to the right. **b**, Quantification of baseline calcium in the genotypes shown in a. N = 5–6 larvae per genotype. Unpaired t-test, p = 0.012. **c**, Crawling deficiency of Tmep knockdown larvae can be restored by knockdown of IPTR, RyR, or by over-expression of NMNAT. Female data is shown. One-way ANOVA with Sidak's multiple comparison correction was used to calculate p values as follows: p = 0.014 (Vglut vs Tmep RNAi), p = 0.0014 (Tmep RNAi vs Tmep/RyR), p < 0.0001 (Tmep RNAi vs Tmepi/ITPRi or NMNAT). **d**, Individual RNAi expression of IPTR, RyR, or UAS-NMNAT does not change baseline contraction rates (for all, p>0.05). Female data is shown. **e**, Model for Tmep influence on presynaptic calcium, synaptic activity, synaptic structure, and locomotion.

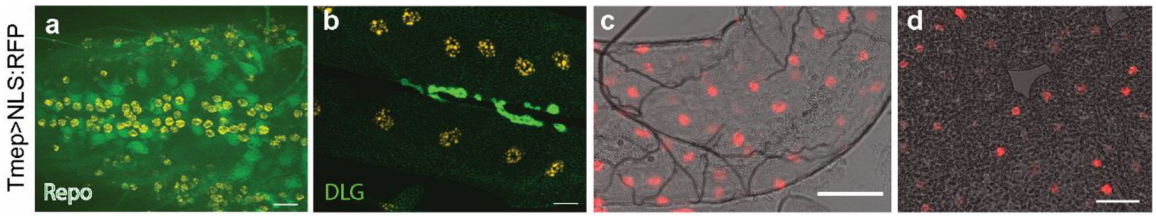

Online Resource 1. Tmep is expressed broadly throughout the larvae.
RedStinger:NLS (red and orange) shows nuclei of cells in which endogenous Tmep is expressed. **a**, Ventral nerve cord. Green is Repo (glial nuclei). **b**, Neuromuscular junction. Green is *discs large* (DLG). **c**, Gut expression. **d**, Fat body expression. For all figures, scale bars = 20 μm.